

# Nano LDL Drug Delivery Systems of Triazole Derivatives: Synthesis, Characterization, Anticancer Evaluation and *In silico* Investigation Targeting HER2 and $\beta$ -Tubulin Proteins

Laila A. Jaragh-Alhadad\*

Department of Chemistry, Kuwait University, Kuwait City, Kuwait

## ABSTRACT

In medicinal chemistry, the 1,2,4-triazole scaffold has a wide spectrum of applications. Using this scaffold to synthesize new derivatives as anticancer agents targeting proliferation proteins like HER2 and  $\beta$ -tubulin and delivered by nano-LDL particles to specific sites is an attractive approach. The 1,2,4-triazole derivatives were fully characterized, an x-ray single crystal confirmed the structure of agent 4f and the morphologies were studied to prove the particles' nano size. The agents were encapsulated into nano-LDL particles, to benefit from the lipid metabolic pathway and the nano-particle size showed an increase after encapsulation. The biological results in the present study showed that 1,2,4-triazole derivatives have anticancer activity toward both breast (MDA468) and prostate (DU145) cancer cell lines. The molecular docking technique was used to predict the potent  $\beta$ -tubulin inhibitor and the scores of eight synthesized compounds were investigated. Biological evaluation and the *insilico* investigation results were parallel. The results showed that agent 4f was the potent triazole derivative with chlorine substituent that possesses the activity toward both cancer cell lines in the range of  $1.23 \pm 0.18$  and  $1.20 \pm 0.78$   $\mu$ M, respectively. In the DU145 cell line cancer cell death was through targeting both HER2 receptor and  $\beta$ -tubulin proteins, while in MDA468 the inhibition was through targeting only tubulin as proved in western blot assessment because MDA468 is HER2 negative receptor. In addition, the docking results revealed that the eight agents targeting  $\beta$ -tubulin, specifically agent 4f has an outstanding score of -5.9 kcal/mol compared with doxorubicin (calc. -6.8 kcal/mol). In sum, 1,2,4-triazole derivatives showed potent anticancer activity targeting HER2 receptor protein and  $\beta$ -tubulin cellular protein in one shot.

**Keywords:** Triazole scaffold derivatives;  $\beta$ -tubulin; HER2; MDA468; DU145; Molecular docking

## INTRODUCTION

Cancer is the second leading cause of death after cardiovascular diseases in the globe. These days, many anticancer agents are approved by the Food and Drug Administration (FDA). However, drug toxicity and resistance of cancer toward chemotherapy and anticancer agents are still the main problems faced. Doxorubicin is a known chemotherapeutic agent used and has harmful effects on the heart and liver. In addition, cisplatin is a commonly used anticancer drug and causes serious problems like resistance, nephrotoxicity and neurotoxicity. All these findings urgently require the investigation of new anticancer drugs with high efficacy, low toxicity and side effects [1].

Tubulin is the building block of the microtubule, which is an important structural protein for the cell involved in cell movement, shape, maintenance and cell division. Cancer cells rely on this protein to divide and this function is high in cancer cells than healthy cells. Therefore, targeting this protein is attractive for future cancer therapy.

The human epidermal growth factor receptor (HER2) is a transmembrane tyrosine kinase receptor that regulates cell survival, proliferation and migration through kinase signaling pathways. The HER2 receptor is associated with malignant phenotype in different human cancers including breast and prostate cancers. It is important to note that the HER2 receptor

**Correspondence to:** Laila A. Jaragh-Alhadad, Department of Chemistry, Kuwait University, Kuwait City, Kuwait; E-mail: laila.alhadad@ku.edu.kw

**Received:** 19-Feb-2024, Manuscript No. ANO-24-29666; **Editor assigned:** 22-Feb-2024, PreQC No. ANO-24-29666 (PQ); **Reviewed:** 07-Mar-2024, QC No. ANO-24-29666; **Revised:** 27-Mar-2025, Manuscript No. ANO-24-29666 (R); **Published:** 04-Apr-2025, DOI: 10.35248/2167-0250.25.14.351

**Citation:** Jaragh-Alhadad LA (2025) Nano LDL Drug Delivery Systems of Triazole Derivatives: Synthesis, Characterization, Anticancer Evaluation and *In silico* Investigation Targeting HER2 and  $\beta$ -Tubulin Proteins. *Andrology*. 14:351.

**Copyright:** © 2025 Jaragh-Alhadad LA. This is an open-access article distributed under the terms of the Creative Commons Attribution License, which permits unrestricted use, distribution and reproduction in any medium, provided the original author and source are credited.

is over-expressed in the external cellular domain in malignant cells more than in benign cells. Therefore, the blockage of the dimerization of the HER2 receptor will inhibit the downstream signaling pathway and tyrosine kinase activity, making it an attractive protein to target.

Triazole is one of the considerable nitrogen-containing scaffolds in drug discovery. It is a simple structure composed of a five-membered ring heterocyclic structure with three nitrogen atoms and two carbon atoms, that forms 1,2,3-triazole and 1,2,4-triazole isomers as shown in Figure 1. A large number of research were carried out on triazole core especially click chemistry because of its wide pharmaceutical properties such as anti-convulsant, anti-alzheimer, antimicrobial, anti-bacterial, anti-viral, anti-inflammatory and anticancer activities. The 1,2,4-triazole core can influence the lipophilicity, polarity and hydrogen bonding of the molecule and this strength of triazole nucleus is evident from the clinical drugs used nowadays but still we need to find more triazole derivatives with a better scaffold and pharmacokinetic profile [2].

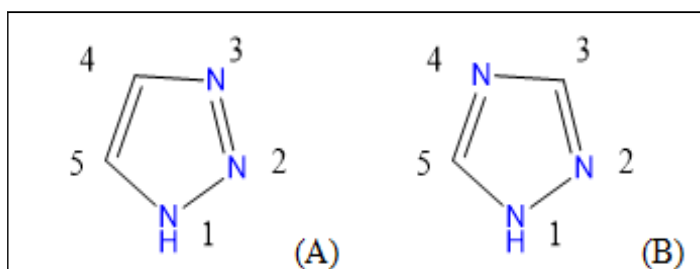


**Figure 1:** The chemical structures of two triazole isomers. A is the 1,2,3-triazole and B is the 1,2,4-triazole.

Several powerful and attractive triazole hybrid molecules were used to have many biological properties in one shot to overcome drug resistance, toxicity and side effects such as 1,2,4-triazole hybrids that possess antibacterial properties, anti-convulsant and anti-depressant activities. Other triazole hybrids found to be Alzheimer's disease inhibitors such as chalcone triazole hybrids and others found to be multi-targets. In addition, benzimidazole and 1,2,4-triazole hybrids were used as antifungal agents. Moreover, quinoline-triazole conjugates possess antiviral activity against SARS-CoV-2. Also, a study reported the importance of triazole core in DNA cleavage activity. Other triazoles elicited anticancer activities by targeting heat shock proteins (HSP27, HSP70, HSP90), EGFR tyrosine kinase and microtubules.

Moreover, various studies targeted cancer cells by drug delivery strategies using triazoles. For example, loading triazole derivatives in nanocomposites for better anti-bacterial and anti-cancer activities. Also, 1,2,4-triazole derivatives nanoparticles were used to target tumor cells and bio-imaging. Further, triazole derivatives were encapsulated in various techniques such as Fe<sub>2</sub>O<sub>3</sub>, copper oxide, zinc oxide nanoparticles and polyethylene glycol conjugate for better drug delivery [3].

Because of all these findings, the triazole scaffold was used to synthesize, characterize and prove the biological activity. Agent 4f structure was confirmed by x-ray crystallography. The 1,2,4-triazole derivatives' morphologies were studied and their particle sizes were confirmed to be in the nanoscale either nano-particles

or nano-rods structures. Then, the derivatives were encapsulated into nano-LDL particles as an active targeting delivery vehicle against both breast (MDA468) and prostate (DU145) cancer cell lines as shown in Figure 2. Western blot assessment showed that the MDA468 cell line is HER2 negative while the DU145 cell line is HER2 positive. This strategy increases cancer cell death in the DU145 cell line by benefiting from the LDL metabolism through binding to LDL receptors and entering the middle of the cancer cell causing cell death. Noting that LDL-receptors are highly expressed in HER2-positive cancer cells more than benign cells. On the other hand, in the MDA468 cell line, the cell death was through  $\beta$ -tubulin protein only. Further, the insilico investigations revealed that all agents targeting  $\beta$ -tubulin especially agent 4f had the most potent score compared to doxorubicin. In sum, benefiting from the active drug to target dual proteins at one time is an attractive idea.

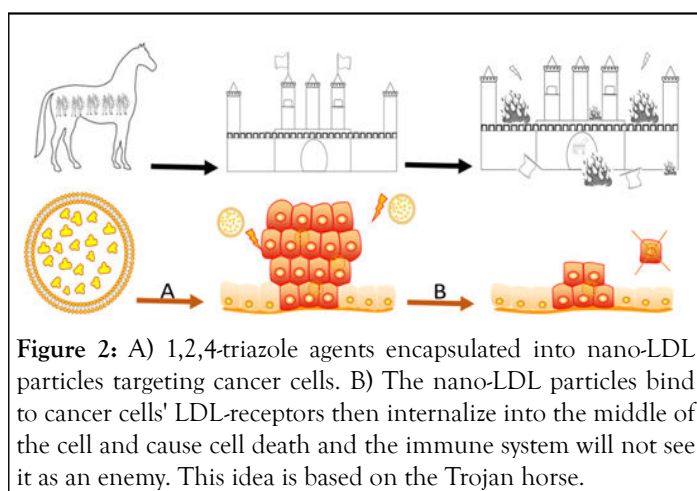


**Figure 2:** A) 1,2,4-triazole agents encapsulated into nano-LDL particles targeting cancer cells. B) The nano-LDL particles bind to cancer cells' LDL-receptors then internalize into the middle of the cell and cause cell death and the immune system will not see it as an enemy. This idea is based on the Trojan horse.

## MATERIALS AND METHODS

### Chemicals

All chemicals and solvents used for the agent's synthesis were commercially available from Sigma Aldrich and Merck companies and were used directly without the need for any further preparation. Chemical synthesis was conducted at the Kuwait University laboratory. Thin layer chromatography (TLC pre-coated aluminum plate silica gel-Merk 9385) was used to monitor the endpoints of the reactions under ultraviolet light at 254 and 350 nm with hexane/ethyl acetate petroleum ether solvent (2:1). Column chromatography was performed using silica gel 60A mesh size 40  $\mu$ M-60  $\mu$ M. The samples' molecular weights were confirmed by mass spectroscopy and were determined by using VG Auto spec QMS 30 and MSg (AEI) spectrometer with EI (70 eV) mode. In addition, triazole derivatives' melting point was also investigated using Stuart's electrothermal melting point apparatus. The <sup>1</sup>H NMR (600 MHz) and <sup>13</sup>C NMR (150 MHz) were measured in a Bruker DPX instrument ( $\delta$  ppm), in DMSO and CDCl<sub>3</sub>, respectively. The triazole agents were mixed and ground with KBr in a disc until became a fine powder. Then, inserted into the device for measurement FTIR-6300 type A range (200 cm<sup>-1</sup>-4000 cm<sup>-1</sup>) and shows absorbance stretching and bending vibrations peaks for each and specific function groups. The UV-VIS. spectra of the

complexes were recorded on Cary 5 UV-VIS Spectrophotometer, Varian (200 nm-900 nm) [4].

## Biology

Breast (MDA468) and prostate (DU145) cancer cell lines were purchased from Cleveland Clinic-Lerner Research Institute-core facility. Cell culture media DMEM, FBS and PBS were from the medial core facility at Lerner Research Institute-Cleveland Clinic. 3-(4, 5-dimethylthiazol-2-yl)-2,5-diphenyl-2H-tetrazolium bromide (MTT), obtained from Sigma-Aldrich (Milwaukee, WI).

## Methods

**General syntheses of 1,2,4-triazole-3-thiol derivatives 4a-h:** Our approach starts with the reaction of benzoate derivative the methyl-2-cyanoacetate 1a-h with hydrazine monohydrate to form hydrazide derivatives 2a-h. The potassium hydroxide base (30 mmol) was dissolved in 20 ml of methanol solvent and stirred for ten minutes. Then hydrazide derivatives 2a-h (20 mmol) were added. After 15 min C<sub>2</sub>S (30 mmol) was added and the reaction mixture was stirred for three hours. After that, 100 ml of diethyl ether was added to form intermediates 3a-h, which were filtered and washed with diethyl ether. The intermediates 3a-h were mixed with hydrazine monohydrate (32 mmol) and the solution was refluxed for one hour. After cooling, the solution was poured into ice water and then neutralized with hydrochloric acid. The solid obtained was recrystallized from methanol to form 1,2,4-triazole-3-thiol derivatives 4a-h in good yields. Structure-Activity Relationship (SAR) was applied to the main skeleton of the 1,2,4-triazole core keeping all branches with the same moieties and changing only one position with different R substituents as shown in Table 1 [5].

**4-Amino-5-phenyl-4H-1,2,4-triazole-3-thiol 4a:** Yield 93%; m.p. 200°C-201°C; Anal. Calcd for C<sub>8</sub>H<sub>8</sub>N<sub>4</sub>S: C, 49.98; H, 4.19; N, 29.14; S, 16.68. Found: C, 49.96; H, 4.20; N, 29.24; S, 16.70.; FTIR (KBr, cm<sup>-1</sup>): 3109, 3054 (NH<sub>2</sub>), 2941 (SH); EI-HRMS: m/z=192.0465 (MH<sup>+</sup>); C<sub>8</sub>H<sub>8</sub>N<sub>4</sub>S requires: m/z=192.0464 (MH<sup>+</sup>); <sup>1</sup>H NMR (400 MHz, DMSO-d<sub>6</sub>): δ=5.79 (s, 2H, NH<sub>2</sub> D<sub>2</sub>O exchangeable), 7.52-8.03 (m, 5H, Ar-CH), 13.93 (s, 1H, SH); <sup>13</sup>C NMR (100 MHz, DMSO-d<sub>6</sub>): δ=166.8, 149.4, 130.4, 128.4 (2C), 128.0 (2C), 125.7. MS: m/z (%) 192 (M<sup>+</sup>, 100), 161 (10), 103 (20), 90 (10), 76 (20), 58 (15).

**4-amino-5-(4-chlorophenyl)-4H-1,2,4-triazole-3-thiol 4b:** Yield 89%; m.p. 207°C-209°C; Anal. Calcd for C<sub>8</sub>H<sub>7</sub>ClN<sub>4</sub>S: C, 42.39; H, 3.11; N, 24.72; S, 14.15; Cl, 15.64. Found: C, 42.40; H, 3.21; N, 24.74; S, 14.25; Cl, 15.65; FTIR (KBr, cm<sup>-1</sup>): 3147, 3100 (NH<sub>2</sub>), 2933 (SH); EI-HRMS: m/z=226.0075 (MH<sup>+</sup>); C<sub>8</sub>H<sub>7</sub>ClN<sub>4</sub>S requires m/z=226.0074 (MH<sup>+</sup>); <sup>1</sup>H NMR (400 MHz, DMSO-d<sub>6</sub>): δ=5.79 (s, 2H, NH<sub>2</sub> D<sub>2</sub>O exchangeable), 7.58 (d, 2H, J=8, Ar-CH), 8.05 (d, 2H, J=8, Ar-CH), 13.97 (s, 1H, SH); <sup>13</sup>C NMR (100 MHz, DMSO-d<sub>6</sub>): δ=167.1, 148.4, 135.2, 129.6 (2C), 128.6 (2C), 124.5. MS: m/z (%) 226 (M<sup>+</sup>, 100), 195 (10), 155 (40), 138 (25), 101 (20), 88 (10), 59 (20).

**4-amino-5-(2-bromophenyl)-4H-1,2,4-triazole-3-thiol 4c:** Yield 92%; m.p. 213°C-215°C; Anal. Calcd for C<sub>8</sub>H<sub>7</sub>BrN<sub>4</sub>S: C, 35.44; H, 2.60; N, 20.66; S, 11.88; Br, 29.47. Found: C, 35.52; H, 2.68; N, 20.67; S, 11.90; Br, 29.49; FTIR (KBr, cm<sup>-1</sup>): 3438, 3293

(NH<sub>2</sub>), 3099 (SH); EI-HRMS: m/z=269.9567 (MH<sup>+</sup>); C<sub>8</sub>H<sub>7</sub>BrN<sub>4</sub>S requires: m/z=269.9569 (MH<sup>+</sup>); <sup>1</sup>H NMR (400 MHz, DMSO-d<sub>6</sub>): δ=5.48 (s, 2H, NH<sub>2</sub> D<sub>2</sub>O exchangeable), 7.49-7.87 (m, 4H, Ar-CH), 13.96 (s, 1H, SH); <sup>13</sup>C NMR (100 MHz, DMSO-d<sub>6</sub>): δ=166.5, 150.0, 134.3, 132.7 (2C), 127.5 (2C), 123.1. MS: m/z (%) 270 (M<sup>+</sup>, 100), 258 (45), 225 (20), 196 (60), 158 (30), 117 (10), 89 (40), 74 (30).

**4-amino-5-(o-tolyl)-4H-1,2,4-triazole-3-thiol 4d:** Yield 91%; m.p. 134°C-135°C; Anal. Calcd for C<sub>9</sub>H<sub>10</sub>N<sub>4</sub>S: C, 52.41; H, 4.89; N, 27.16; S, 15.55. Found: C, 52.44; H, 4.90; N, 27.19; S, 15.65.; FTIR (KBr, cm<sup>-1</sup>): 3436, 3288 (NH<sub>2</sub>), 3105 (SH); EI-HRMS: m/z=206.0620 (MH<sup>+</sup>); C<sub>9</sub>H<sub>10</sub>N<sub>4</sub>S requires: m/z=206.0620 (MH<sup>+</sup>); <sup>1</sup>H NMR (400 MHz, DMSO-d<sub>6</sub>): δ=2.50 (s, 3H, CH<sub>3</sub>), 5.77 (s, 2H, NH<sub>2</sub> D<sub>2</sub>O exchangeable), 7.34-7.83 (m, 4H, Ar-CH), 13.90 (s, 1H, SH); <sup>13</sup>C NMR (100 MHz, DMSO-d<sub>6</sub>): δ=167.2, 149.9, 138.2, 129.8 (2C), 126.8 (2C), 123.7, 21.4. MS: m/z (%) 206 (M<sup>+</sup>, 100), 192 (40), 132 (40), 118 (30), 91 (30).

**4-amino-5-(4-methoxyphenyl)-4H-1,2,4-triazole-3-thiol 4e:** Yield 95%; m.p. 227°C-228°C; Anal. Calcd for C<sub>9</sub>H<sub>10</sub>N<sub>4</sub>OS: C, 48.63; H, 4.53; N, 25.21; S, 14.43. Found: C, 48.66; H, 4.51; N, 25.25; S, 14.51; FTIR (KBr, cm<sup>-1</sup>): 3437, 3309 (NH<sub>2</sub>), 3140 (SH); EI-HRMS: m/z=222.0570 (MH<sup>+</sup>); C<sub>9</sub>H<sub>10</sub>N<sub>4</sub>OS requires: m/z=222.0570 (MH<sup>+</sup>); <sup>1</sup>H NMR (400 MHz, DMSO-d<sub>6</sub>): δ=3.21 (s, 3H, CH<sub>3</sub>), 5.76 (s, 2H, NH<sub>2</sub> D<sub>2</sub>O exchangeable), 7.08 (d, 2H, J=8, Ar-CH), 7.98 (d, 2H, J=8, Ar-CH), 13.80 (s, 1H, SH); <sup>13</sup>C NMR (100 MHz, DMSO-d<sub>6</sub>): δ=166.4, 160.8, 149.2, 129.5 (2C), 118.0, 113.9 (2C), 55.3. MS: m/z (%) 222 (M<sup>+</sup>, 100), 208 (5), 177 (5), 151 (40), 134 (300), 119 (10), 90 (10), 60 (10).

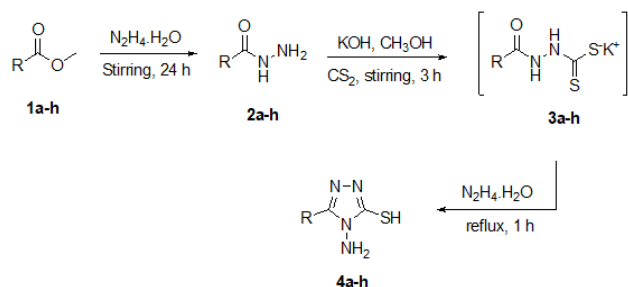
**4-amino-5-(2-chlorophenyl)-4H-1,2,4-triazole-3-thiol 4f:** Yield 85%; m.p. 178°C-180°C; Anal. Calcd for C<sub>8</sub>H<sub>7</sub>ClN<sub>4</sub>S: C, 42.39; H, 3.11; N, 24.72; S, 14.15; Cl, 15.64. Found: C, 42.41; H, 3.20; N, 24.72; S, 14.24; Cl, 15.66; FTIR (KBr, cm<sup>-1</sup>): 3152, 3101 (NH<sub>2</sub>), 2935 (SH); EI-HRMS: m/z=226.0073 (MH<sup>+</sup>); C<sub>8</sub>H<sub>7</sub>ClN<sub>4</sub>S requires: m/z=226.0074 (MH<sup>+</sup>); <sup>1</sup>H NMR (400 MHz, DMSO-d<sub>6</sub>): δ=5.52 (s, 2H, NH<sub>2</sub> D<sub>2</sub>O exchangeable), 7.48-7.65 (m, 4H, Ar-CH), 13.97 (s, 1H, SH); <sup>13</sup>C NMR (100 MHz, DMSO-d<sub>6</sub>): δ=166.7, 148.9, 133.3, 132.5, 132.3, 129.6, 127.1, 125.2. MS: m/z (%) 226 (M<sup>+</sup>, 100), 195 (10), 105 (10), 155 (20), 138 (25), 101 (20), 59 (15).

**4-amino-5-methyl-4H-1,2,4-triazole-3-thiol 4g:** Yield 91%; m.p. 215°C-216 °C; Anal. Calcd for C<sub>3</sub>H<sub>6</sub>N<sub>4</sub>S: C, 27.68; H, 4.65; N, 43.04; S, 24.63. Found: C, 27.69; H, 4.66; N, 43.06; S, 24.66; FTIR (KBr, cm<sup>-1</sup>): 3176, 3111 (NH<sub>2</sub>), 2948 (SH); EI-HRMS: m/z=130.0307 (MH<sup>+</sup>); C<sub>3</sub>H<sub>6</sub>N<sub>4</sub>S requires: m/z=130.0308 (MH<sup>+</sup>); <sup>1</sup>H NMR (400 MHz, DMSO-d<sub>6</sub>): δ=2.23 (s, 3H, CH<sub>3</sub>), 5.51 (s, 2H, NH<sub>2</sub> D<sub>2</sub>O exchangeable), 13.38 (s, 1H, SH); <sup>13</sup>C NMR (100 MHz, DMSO-d<sub>6</sub>): δ=165.3, 149.1, 10.3. MS: m/z (%) 130 (M<sup>+</sup>, 100), 98 (15), 59 (15).

**2-(4-amino-5-mercapto-4H-1,2,4-triazol-3-yl)acetonitrile 4h:** Yield 95%; m.p. 207°C-209°C; Anal. Calcd for C<sub>4</sub>H<sub>5</sub>N<sub>5</sub>S: C, 30.96; H, 3.25; N, 45.13; S, 20.66. Found: C, 30.70; H, 3.23; N, 45.11; S, 20.69; FTIR (KBr, cm<sup>-1</sup>): 3170, 3127 (NH<sub>2</sub>), 3020 (SH); EI-HRMS: m/z=155.0258 (MH<sup>+</sup>); C<sub>4</sub>H<sub>5</sub>N<sub>5</sub>S requires: m/z=155.0260 (MH<sup>+</sup>); <sup>1</sup>H NMR (400 MHz, DMSO-d<sub>6</sub>): δ=5.51 (s, 2H, NH<sub>2</sub> D<sub>2</sub>O exchangeable), 8.4 (s, 2H), 13.62 (s, 1H, SH); <sup>13</sup>C

NMR (100 MHz, DMSO-d<sub>6</sub>):  $\delta$ =165.7, 142.1. MS:  $m/z$  (%) 155 ( $M^+$ , 10), 115 (100), 70 (5), 57(15).

**Table 1:** The eight synthesized 1,2,4-triazole derivatives.



Agent no.	R=	Yield %
4a	C <sub>6</sub> H <sub>5</sub>	93%
4b	4-ClC <sub>6</sub> H <sub>4</sub>	89%
4c	2-BrC <sub>6</sub> H <sub>4</sub>	92%
4d	3-CH <sub>3</sub> C <sub>6</sub> H <sub>4</sub>	91%
4e	4-OCH <sub>3</sub> C <sub>6</sub> H <sub>4</sub>	95%
4f	2-ClC <sub>6</sub> H <sub>4</sub>	85%
4g	CH <sub>3</sub>	91%
4h	CH <sub>2</sub> CN	95%

### Agent 4f single-crystal data collection and structure refinement

The crystal structure of agent 4f was grown by dissolving 15.0 mg of it in one ml of hot ethanol, then, the solution was covered with parafilm and small holes were made in it to allow slow evaporation. After a week we got a suitable crystal for diffraction. The single crystal data analysis was made by a Bruker SHELXTL Software Package using a narrow-frame algorithm. Data were corrected for absorption effects using the Multi-Scan method (SADABS). The ratio of minimum to maximum apparent transmission was 0.571. The calculated minimum and maximum transmission coefficients (based on crystal size) are 0.1970 and 0.5840 [6].

### The triazole agents' morphology investigation by SEM

The eight triazole derivatives' surface morphology was determined by taking five micrograms of the dry powder and placing them on carbon tape on a stub. Then, coated with platinum in a sample coating machine before Scanning Electron Microscope (SEM) reading at 15.0 kV. Five SEM readings were taken at different magnifications X50, X100, X500, X1000 and X2000 using (JEOL-EDS) system.

### Thermogravimetric Analysis (TGA) of the triazole agents

TGA is a technique used to measure the sample when heated and cooled, to monitor the weight loss and changes that happened and to check the sample's thermal stability. Triazole samples were loaded into an aluminum pan and heated from 30°C to 800°C on a Shimadzu TGA-60; the nitrogen flow and heating rates were 50 ml/min and 10°C min<sup>-1</sup>, respectively [7].

### Encapsulation of 1,2,4-triazole agents into nano-LDL particles

The structure of the commercially available nano LDL-depleted serum is like the native LDL particles' structure. Therefore, 50  $\mu$ l of the nano-LDL particles were used for encapsulation with five  $\mu$ l of the triazole agent with a ratio of (5:1). The agents were mixed with nano-LDL particles by pipetting, vortexing and sonicating using (A poly-Tron dispersing mixing device made in Switzerland by Kinematica AG). Then, triazole agents were left to reform and reconstruct overnight in a 4°C fridge before taking any measurements.

### Zeta data before and after agents' encapsulation

Briefly, after the 1,2,4-triazole agent's encapsulation into nano-LDL particles, Phosphate Buffer Saline (PBS) was used as our

blank and for washing between each sample run in the zeta sizer device. First, LDL was used as our plain vehicle. Then, 100  $\mu$ l of the agent was dispersed in two ml of a suitable solvent (DMSO) and the size measurements were done using a zeta sizer at pH seven (Nano ZS-Malvern Paralytical Ltd, UK) at the Kuwait University-RSPU facility. This test was used to measure all triazole agents' particle sizes before and after encapsulation with nano-LDL particles. The data were presented as particles' size  $\pm$  standard deviation [8].

### UV-VIS readings

UV-VIS spectrophotometer optical method investigates how light interacts with matter in the UV visible range of light. A sample of a triazole agent and DMSO solvent (blank) were prepared in two Quartz cuvettes and placed in the spectrophotometer (UV-VIS NIR-Agilent Cary 5000). Inside the device, a direct beam of light will pass through the sample and the blank cuvettes and absorb a particular wavelength. In-depth, the light that passes through the blank is fully transmitted while the light of the sample of triazole will not be transmitted (Beer-Lambert light), first light is diffracted and then directed to the detector (PMT-photo multiplier tube). The spectrograph reading shows the absorbance values of the triazole agent that has a range within the ultraviolet and visible regions. These steps were repeated for each agent and recorded within a wavelength range of 300 nm-700 nm Flex Station-Molecular Devices at Lerner Research Institute at Cleveland Clinic. The UV-Vis absorption measurement for each triazole agent was analyzed after centrifugation of the sample and the re-dispersion in distilled water [9].

### Cell proliferation assay and statistical analysis

Breast cancer (MDA468) and prostate cancer (DU145) cells were maintained in DMEM media supplemented with 10% FBS, 1% penicillin/streptomycin and 1% L-Glutathione and incubated in humidified air with 5% CO<sub>2</sub>. FBS is inactivated at a 37°C water bath for 30 minutes before use. The *in-vitro* cell proliferation assay was carried out based on the manufacturer's protocol provided by the WST-1 assay kit.

Briefly,  $5 \times 10^4$  cells/well/ml from the breast and prostate cell lines were seeded on 96-well plates and incubated overnight. The cells were treated with 100  $\mu$ l of various concentrations of nano-LDL particles encapsulated with triazole agents and incubated for 48 hr. Then, ten  $\mu$ l WST-1 reagent was added to each well. The amount of the formazan product formed was determined by measuring the absorbance at a wavelength of 440 nm using a plate reader (SoftMax Pro 9.0 Flex Station-Molecular Devices) at lerner research institute at Cleveland clinic. The experiments were performed in quadruplicate concentrations.

Graph pad prism 09 was used for statistical analysis. All *in-vitro* data were presented as the mean  $\pm$  standard error. The statistical significance was defined as p values < 0.05.

## Western blotting analysis targeting HER2 in MDA468 and DU145 cell lines

Confluent cancer cell monolayer dishes (MDA468 and DU145) were washed with PBS and harvested by the scraper. The supernatants were then removed after centrifugation and the collected cell pellets were lysed by mixing them with RIPA, PI and EDTA 150  $\mu$ L. The cells were then vortexed and centrifuged for one hour. Cell lysates were normalized using polyacrylamide gel electrophoresis in the presence of 0.1% SDS. The gel was transferred to the membrane followed by blocking with NFDm and PBST. The membrane was washed 3-4 times with PBST for five minutes. Then, the membrane was incubated with the primary antibody (targeting HER2, rabbit 1:1,000 dilution) overnight. On the next day, the membrane was washed 3-4 times with PBST and incubated with the secondary antibody (anti-rabbit HRP antibody 1:1,000 dilution) for one hour. The membrane was again washed with PBST 3-4 times to be prepared for the visualization of the bands by chemiluminescence, where B-actin was the housekeeping control.

### *In silico* study preparation and interactions of triazole agents

In the present study, docking was performed to evaluate the binding modes of all designed triazole derivatives and the possible interactions with the binding pocket of the  $\beta$ -tubulin protein. The data were retrieved from the Protein Data Bank (PDB). The structures of 1,2,4-triazole derivatives were drawn and saved in mol in Maestro (Schrodinger, LLC, New York, NY, USA). Each structure was assigned for an appropriate bond order using the LigPrep package from Schrodinger (LLC, NY, USA). The ligands were converted to Maestro format, optimized and computed partial atomic charges. Then, at most, 32 poses per ligand were generated with different steric features for the subsequent docking study. The automatic protein-ligand interactions docking diagram was generated to provide hydrogen bonds and hydrophobic contacts. Docking scores were calculated, the more negative the energy ( $\Delta G_o$ ) represented the effective binding and hence the activity of the triazole agent [10].

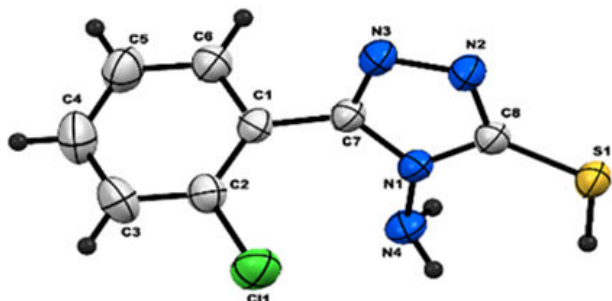
## RESULTS

### Crystal structure of agent f4

All agents were synthesized and well-characterized, agent 4f structure was confirmed by x-ray crystallography, the crystal data and structure refinement are summarized in Table 2, while the bond lengths and angles are in Table 3. The data showed that agent 4f has a clear colorless block with the formula C<sub>8</sub>H<sub>7</sub>ClN<sub>4</sub>S and has a molecular weight of 226.69. It belongs to an orthorhombic system with (P 2ac 2ab) space group. The estimated cell parameters are a=5.5575(3) Å, b=12.0158(6) Å, c=30.3978(15) Å,  $\alpha=90^\circ$ ,  $\beta=90^\circ$ ,  $\gamma=90^\circ$ . The S1-C8 bond length (1.682 Å) is within the value of the C-S single bond. The bond length of C11-C2 is (1.735 Å). The delocalization of electrons by resonance in chlorobenzene is attributed to partial double bond character due to which bond length is shorter than a single

bond of the  $sp^2$  hybridization. The bond lengths of N2-N3 and N1-N4 are almost equal (1.382 and 1.399 Å) and are within the value of a single bond.

**Table 2:** Structural parameters of agent 4f.



Parameter	4f
Formula weight	226.69
Chemical formula	$C_8H_7N_4SCl$
Temperature	296(2) K
Wavelength	Cu $K\alpha$ ( $\lambda=1.54178$ Å)
Crystal system	Orthorhombic
Crystal size	0.210 × 0.160 × 0.120 mm
Crystal habit	Colorless block
Space group	$P 2_1 c 2_1 b$
<b>Unit cell dimensions</b>	
a (Å)	5.5575(3)
b (Å)	12.0158(6)
c (Å)	30.3978(15)
$\alpha$ (°)	90
$\beta$ (°)	90
$\gamma$ (°)	90
Density ( $g/cm^3$ )	1.484
F(000)	928
$\theta$ range for data collection (°)	2.907 to 66.583
Volume (Å <sup>3</sup> )	2029.90(18)
Z	8
Absorption coefficient ( $mm^{-1}$ )	0.69

Measured reflections	7845
Independent reflections	3787 (R(int)=0.0478)
Observed reflections	1380
Refinement method	'\f and \w scans'
Final R indices (observed data)	R1=0.0372, wR2=0.1080
R indices (all data)	R1=0.0378, wR2=0.1087
Goodness-of-fit on F2	1.1
Largest diff. peak and hole (eÅ <sup>-3</sup> )	0.239 and -0.269

**Table 3:** Agent 4f bond lengths and angles.

Bond lengths (Å)		Bond angles (Å)	
N2-C8	1.337(3)	C8-N2-N3	113.15(16)
N2-N3	1.382(2)	C8-N1-C7	108.22(16)
N1-C8	1.370(2)	C8-N1-N4	127.28(16)
N1-C7	1.377(2)	C7-N1-N4	123.85(16)
N1-N4	1.399(2)	C8-S1-H1	109.5
S1-C8	1.6821(18)	C6-C1-C2	118.51(19)
S1-H1	1.2	C6-C1-C7	119.11(18)
C1-C6	1.388(3)	C2-C1-C7	122.31(19)
C1-C2	1.394(3)	C3-C2-C1	120.8(2)
C1-C7	1.469(3)	C3-C2-C11	119.07(18)

### Triazole agent's morphology

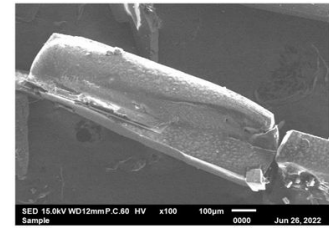
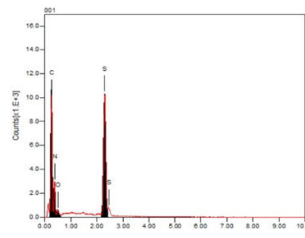
SEM images were taken for the eight triazole derivatives and the morphological characterization of them revealed uniform morphologies. In-depth, Triazole agents 4b, 4c and 4g showed nano sheets structures while agents 4a, 4d, 4e, 4f and 4h showed rode-like structures as shown in Table 4. These nanostructures are very important and affect the drug delivery strategy that causes biological activity and cell death. The sheet structures are important to cover a big area in the middle of the cancer cell

and the rode-like structures both disrupt the tubulin division processes and the HER2 receptor downstream signaling pathways. All these findings showed the nano size of the triazole agents leads to potent biological activity [11].

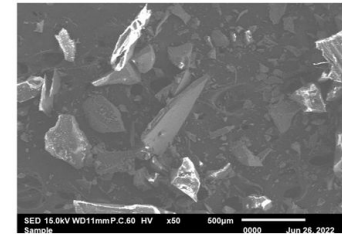
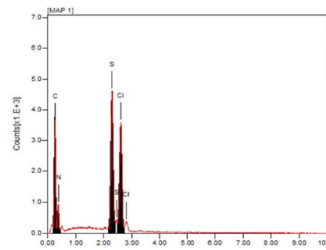
**Table 4:** Triazole agents' elemental presence in the sample with the morphological shapes. The SEM micrographs of the agents were observed and generally were smooth surfaces without holes or cracks viewed at different magnifications and showed nanosheets and nanorod structures.

Agent	Elements present in the sample	Agents morphology
-------	--------------------------------	-------------------

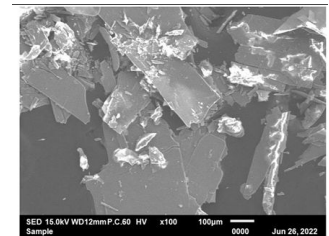
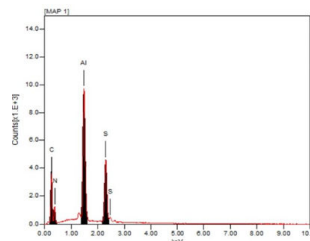
4a



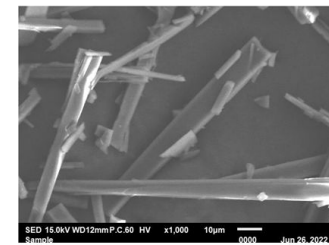
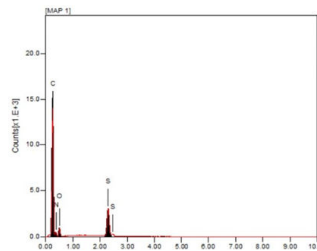
4b



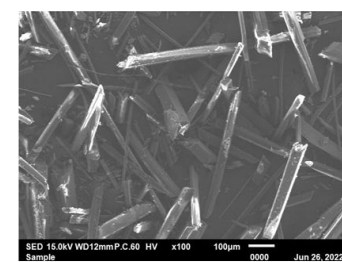
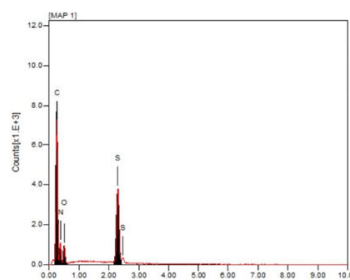
4c



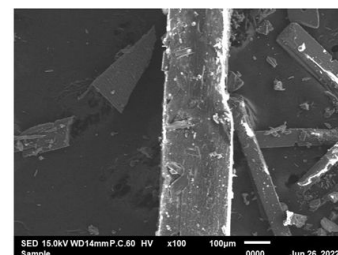
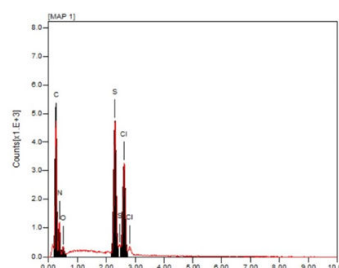
4d



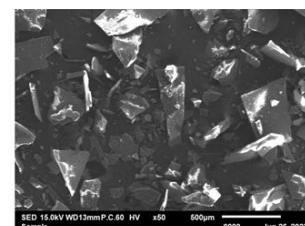
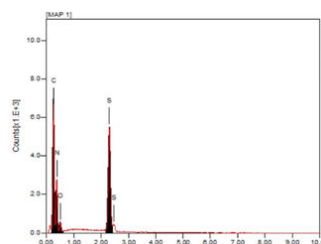
4e



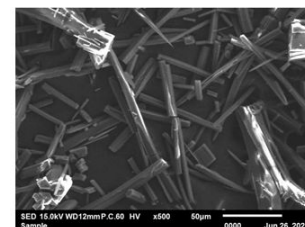
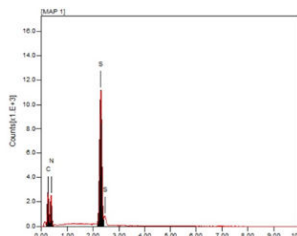
4f



4g



4h



### The thermal stability of triazole derivatives

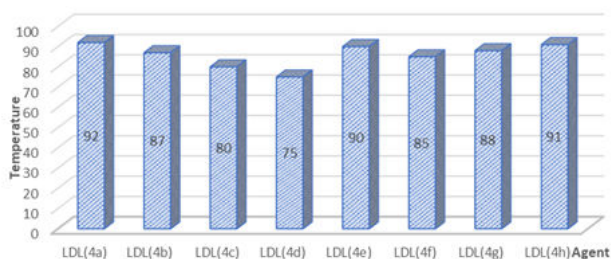
The thermal stability of the nano-LDL particles encapsulated with triazole derivatives was analyzed by TGA. TGA curves showed weight loss and the analysis was measured in the range of 25°C to 800°C as summarized in Table 5. The TGA Analysis showed that all triazole derivatives have two steps of decomposition, the first step starts at 80°C-200°C where the whole compound is decomposed, leaving the NH<sub>2</sub> group. Then, the NH<sub>2</sub> group is eliminated in the second step at 200-800. Comparing the decomposition results of each triazole derivative

before and after encapsulation with nano-LDL particles, we found that nano-LDL particles loaded with triazole agent generally decomposed at low temperatures while the agent itself decomposed at higher temperatures. These findings were noticed for all eight triazole agents [12]. Recently, Haolong et al., proved in their research analyzing the LDL/agents thermal gravimetric results, that LDL had a small mass loss below 280°C which supports our findings.

**Table 5:** TGA analysis for nano-LDL particles encapsulated with triazole agents.

LDL loaded agent	Temp. (°C)	Weight loss (%) Found (calcd.)	Assignment
4a C <sub>8</sub> H <sub>8</sub> N <sub>4</sub> S	92-200	93.84 (91.66)	Elimination of C <sub>8</sub> H <sub>6</sub> N <sub>3</sub> S
	200-800	6.16 (8.33)	Elimination of NH <sub>2</sub>
4b C <sub>8</sub> H <sub>7</sub> ClN <sub>4</sub> S	87-200	92.22 (92.92)	Elimination of C <sub>8</sub> H <sub>5</sub> ClN <sub>3</sub> S
	800	7.88 (7.49)	Elimination of NH <sub>2</sub>
4c C <sub>8</sub> H <sub>7</sub> BrN <sub>4</sub> S	80-200	90.42 (88.92)	Elimination of C <sub>8</sub> H <sub>5</sub> BrN <sub>2</sub> S
	200-800	5.36 (5.90)	Elimination of NH <sub>2</sub>
	>800	4.22 (5.16)	Remaining N

4d C <sub>9</sub> H <sub>10</sub> N <sub>4</sub> S	75-195	90.25 (92.22)	Elimination of C <sub>9</sub> H <sub>8</sub> N <sub>3</sub> S
	200-800	7.00 (7.75)	Elimination of NH <sub>2</sub>
4e C <sub>9</sub> H <sub>10</sub> N <sub>4</sub> OS	90-200	91.12 (92.68)	Elimination of C <sub>9</sub> H <sub>8</sub> N <sub>3</sub> OS
	200-800	8.88 (7.19)	Elimination of NH <sub>2</sub>
4f C <sub>8</sub> H <sub>7</sub> ClN <sub>4</sub> S	85-200	92.59 (92.92)	Elimination of C <sub>8</sub> H <sub>7</sub> ClN <sub>4</sub> S
	200-800	7.08 (7.06)	Elimination of NH <sub>2</sub>
4g C <sub>3</sub> H <sub>6</sub> N <sub>4</sub> S	88-200	91.85 (89.22)	Elimination of C <sub>3</sub> H <sub>6</sub> N <sub>3</sub> S
	200-800	8.15 (10.75)	Elimination of N
4h C <sub>4</sub> H <sub>5</sub> N <sub>5</sub> S	91-200	93.31 (90.32)	Elimination of C <sub>4</sub> H <sub>4</sub> N <sub>4</sub> S
	200-800	6.69 (9.67)	Elimination of NH



### Nano-LDL particles containing triazole agent's characterization

After encapsulation of the 1,2,4-triazole agents into nano-LDL particles, the particle sizes were measured and the data were summarized in Table 6. All nano-LDL particles encapsulated with the triazoles were bigger in particle size than the plain nano-LDL itself. In addition, nano-LDL particles after

encapsulation became bigger than before encapsulation and this proved our loading strategy. The data revealed that agent 4c is the biggest in particle size which had the sheet structure, while agent 4a is the smallest in particle size which had the rode-like structure.

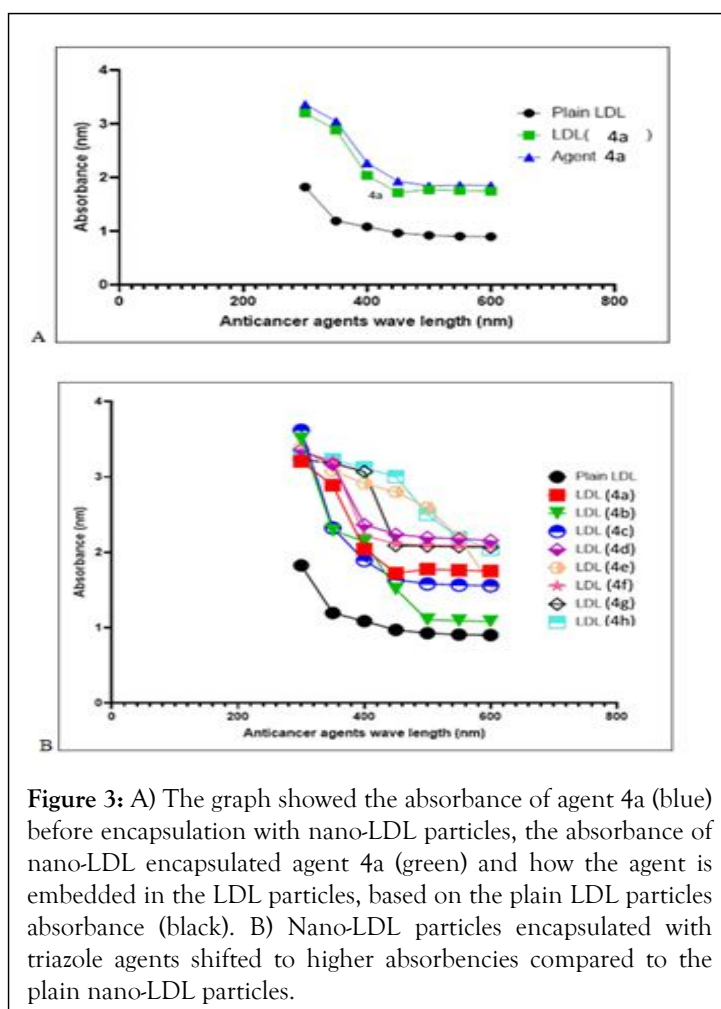
**Table 6:** Triazole agents' size distribution before and after encapsulation with nano-LDL particles.

Agent	Agent size before nano-LDL encapsulation	Agent size after nano LDL encapsulation
Plain LDL*		27.85
4a	306.9 ± 76.39	313.0 ± 22.65
4b	141.8 ± 1.900	436.5 ± 127.2
4c	562.4 ± 72.96	1571 ± 451.2
4d	414.9 ± 150.6	546.9 ± 144.2
4e	180.1 ± 55.04	476.6 ± 72.28
4f	165.9 ± 28.28	395.3 ± 65.99
4g	126.3 ± 7.980	296.5 ± 50.28
4h	322.5 ± 88.26	442.4 ± 77.20

Note: \*The control vehicle

### Triazole derivatives and nano-LDL particle characterizations

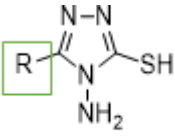
The UV-Vis spectra of plain nano LDL particles showed strong absorption of the electromagnetic waves in the visible region and recorded wavelengths at 300, 350, 400, 450, 500, 550 and 600 nm. In Figure 3A, the graph showed a peak for plain nano-LDL particles and a shifted peak to higher absorbencies for triazole agent 4a and in the middle is the peak for nano-LDL particles encapsulated with triazole agent 4a which became heavier and had a new absorbance peak. On another meaning, this proved the encapsulation of the agent into nano-LDL particles. The graph in Figure 3B showed that all nano-LDL particles encapsulated with the triazole derivatives shifted to higher absorbencies than the plain nano-LDL particle peak in the black color [13].

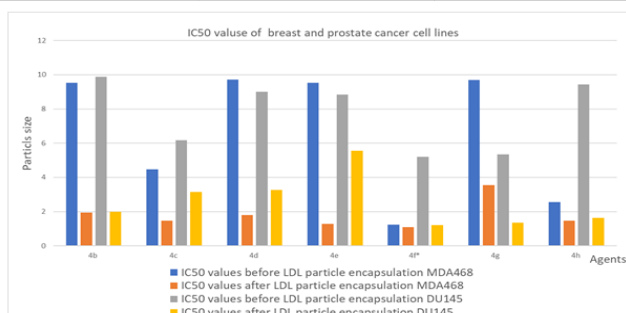


### Cell proliferation assessments before and after treatment with nano-LDL particles encapsulated triazole agents

The proliferation assay of the 1,2,4-triazole agents against both MDA468 and DU145 was performed using MTT assay and the results are summarized in Table 7. Nowadays attention has been given to the synthesis of new triazole agents with the capability of killing cancer cells. The biological evaluation confirmed that cancer cell growth is inhibited throughout 48-hour treatment, with no significant toxicity before that. Further, the results showed that all triazole derivatives showed potent anti-cancer activity before and after encapsulation with nano-LDL particles. In addition, the data revealed that our agents target MDA468 more than the DU145 cell line after encapsulation in the ranges of  $(1.15 \pm 0.75$  to  $3.55 \pm 1.12 \mu\text{M})$  and  $(1.20 \pm 0.78$  to  $5.55 \pm 1.16 \mu\text{M})$  respectively. Agent 4g with methyl substituent, showed potent anticancer activity against the prostate cancer cell line more than the breast cancer cell line, in the range of  $1.35 \pm 0.66 \mu\text{M}$  and  $3.55 \pm 1.12 \mu\text{M}$  respectively. Moreover, the IC<sub>50</sub> data showed that the chlorine substituent in the ortho position (4f) is much stronger than in the para position (4b). It is noticeable that 4-amino-5-(2-chlorophenyl)-4H-1,2,4-triazole-3-thiol agent 4f is the most potent triazole derivative with significant toxicity and efficacy in both breast and prostate cancer cell lines before and after nano-LDL encapsulation in both cell lines. In MDA468 cell line cell proliferation inhibition showed IC<sub>50</sub> values range  $1.23 \pm 0.18$  became  $1.15 \pm 0.74 \mu\text{M}$  after encapsulation and in DU145 cell line the growth inhibition was  $5.19 \pm 0.41$  became  $1.20 \pm 0.78$  became after encapsulation respectively. This activity observed to be due to the chloride substituent on the ortho position which binds like a key and locks to the LDL-receptor internalize into the cell and showed biological activity [14]. Generally, cell lines treated with nano-LDL particles encapsulated with anticancer agents showed better IC<sub>50</sub> values than treatment before encapsulations.

**Table 7:** IC<sub>50</sub> data of cancer cell lines treated with nano-LDL particles encapsulated with triazole derivatives.

Agent		IC <sub>50</sub> values before LDL particle encapsulation MDA468	IC <sub>50</sub> values after LDL particle encapsulation MDA468	IC <sub>50</sub> values before LDL particle encapsulation DU145	IC <sub>50</sub> values after LDL particle encapsulation DU145
					
	<b>4a-h</b>				
4a	C <sub>6</sub> H <sub>5</sub>	8.89 ± 1.82	1.20 ± 0.75	7.39 ± 0.63	4.51 ± 0.61
4b	4-ClC <sub>6</sub> H <sub>4</sub>	9.53 ± 0.95	1.94 ± 0.25	9.87 ± 0.94	1.98 ± 0.81
4c	2-BrC <sub>6</sub> H <sub>4</sub>	4.48 ± 0.45	1.47 ± 0.75	6.18 ± 0.93	3.14 ± 1.14
4d	3-CH <sub>3</sub> C <sub>6</sub> H <sub>4</sub>	9.71 ± 0.05	1.79 ± 1.45	9.00 ± 1.12	3.27 ± 0.90
4e	4-OCH <sub>3</sub> C <sub>6</sub> H <sub>4</sub>	9.53 ± 0.74	1.27 ± 0.81	8.83 ± 0.79	5.55 ± 1.16
4f*	2-ClC <sub>6</sub> H <sub>4</sub>	1.23 ± 0.18*	1.15 ± 0.74*	5.19 ± 0.41*	1.20 ± 0.78*
4g	CH <sub>3</sub>	9.69 ± 0.44	3.55 ± 1.12	5.34 ± 1.09	1.35 ± 0.66
4h	CH <sub>2</sub> CN	2.56 ± 1.05	1.47 ± 0.74	9.43 ± 0.55	1.63 ± 1.01



MDA468: Breast cancer cells, DU145: Prostate cancer cells. Agent 4f\*, the most potent agent before and after encapsulation toward both cell lines.

### Western blot assessment of cancer cell lines

The cells were extracted and treated with DMSO, separated by SDS-PAGE then transferred into a nitrocellulose membrane targeting the HER2 protein by primary and secondary antibodies in the presence of B-actin as a control. The potent agents were used to run western blot and target HER2 protein. The data in Figure 4 showed that the DU145 cell line expressing HER2 protein and the triazole derivatives targeted it but did not target the MDA468 cell line which is the HER2 negative. The result proved that agents 4f and 4h reduced cell proliferation only in the DU145 cell line. In-depth, agent 4h is more potent than agent 4f when targeting the DU145 cell line and reduces the band expression. These findings are parallel to what is found in the literature and parallel to the biological and *in silico* results. In short, the MDA468 cell line is the HER2 negative cell line while DU145 is the HER2 positive cell line and the triazole

agents targeted the HER2 receptor in DU145 cancer cell line. From these results, we confirmed that the triazole agents targeted the DU145 cell line through two proteins HER2 and  $\beta$ -tubulin. On the other hand, in the MDA468 cell line the agents targeted only the  $\beta$ -tubulin protein [15].

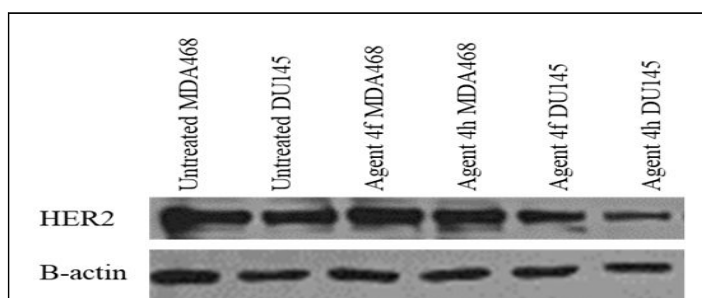


**Figure 4:** Both breast (MDA468) and prostate (DU145) cancer cell lines were used to test the potency of agents 4f and 4h targeting HER2 receptors. The data showed that the agents targeted DU145 the positive HER2 cell line, not MDA468 the HER2 negative cell line. In addition, agent 4h is stronger than 4f when treated with the DU145 cell line.

### *In silico* computations

Therefore, *in silico* investigations were conducted only for the agents targeting the  $\beta$ -tubulin protein which is in both cell lines. The 3D crystal structure of the  $\beta$ -tubulin protein with PDB access code: 1JFF was downloaded and used as a template for all *in silico* estimations. All ions, heteroatoms, inhibitors and water molecules were eliminated for  $\beta$ -tubulin preparation. The protonation state of  $\beta$ -tubulin residues was assigned using PropKa program. The eight synthesized triazole agents were manually constructed and then subjected to molecular minimization using the MMFF94S force field within SZYBKI software. All docking anticipations were conducted with the assistance of AutoDock4.2.6 software. The technical details of the utilized molecular docking technique are described elsewhere. Briefly, the Lamarckian Genetic Algorithm (LGA) was employed for docking computations with the following parameters: 250 independent docking runs and a maximum number of 25,000,000 energy evaluations. The rest docking settings were set at their default values. The grid box size of the  $\beta$ -tubulin protein for the dimensions x, y and z was 50 Å. Auto grid program was employed to create the grid maps with a spacing of 0.375 Å. The grid box was centered on x=0.673, y=-16.448 and z=12.647 Å. The atomic charges of the synthesized compounds using the Gasteiger-Marsili method. The BIOVIA Materials Studio was utilized to visualize all molecular interactions.

### Molecular docking

The performance of AutoDock4.2.6 software in predicting the correct ligand- $\beta$ -tubulin binding mode was assessed. For assessment purposes, the co-crystallized Taxol inhibitor was redocked inside the binding pocket of the  $\beta$ -tubulin protein and the predicted docking pose was compared to the native binding mode (PDB ID: 1JFF) as shown in Figure 5 [16].

As depicted in Figures 6 and 7, the comparison of the anticipated mode obtained from AutoDock4.2.6 software and the native binding mode yielded an RMSD=1.35 . The computed RMSD demonstrated that the anticipated docking pose was like the native binding mode of Taxol. The predicted docking scores and binding features are compiled in Tables 8 and 9 compared to doxorubicin positive control, the data showed that all studied triazole agents revealed good docking scores toward  $\beta$ -tubulin protein with values in the range of -3.7 to -5.9 kcal/mol. The 2D molecular interactions for the eight synthesized compounds are represented in Figure 7. Most of the synthesized compounds participated in the same docking poses, exhibiting H-bonds with the essential residues in the binding pocket like THR276 and other interactions such as vdW pi-based and hydrophobic interactions. Agent 4f demonstrated a superior docking score with a value of -5.9 kcal/mol against the  $\beta$ -tubulin protein. Precisely, agent 4f formed four hydrogen

bonds with THR276 (2.16, 2.47 and 2.07 Å) and PRO274 (2.08 Å).

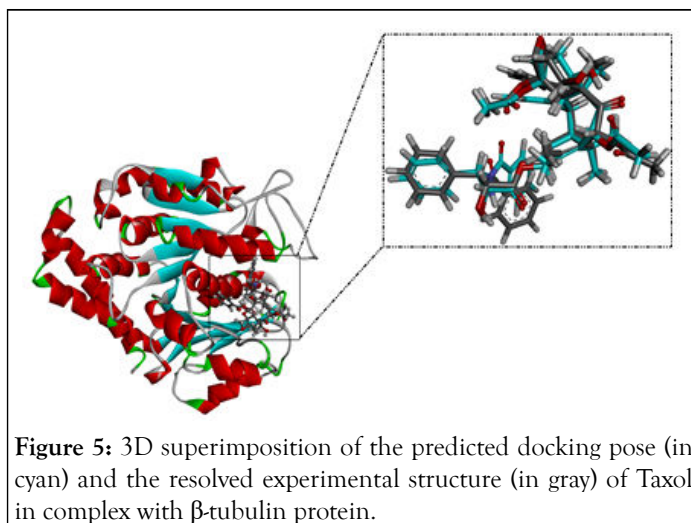


**Figure 5:** 3D superimposition of the predicted docking pose (in cyan) and the resolved experimental structure (in gray) of Taxol in complex with  $\beta$ -tubulin protein.

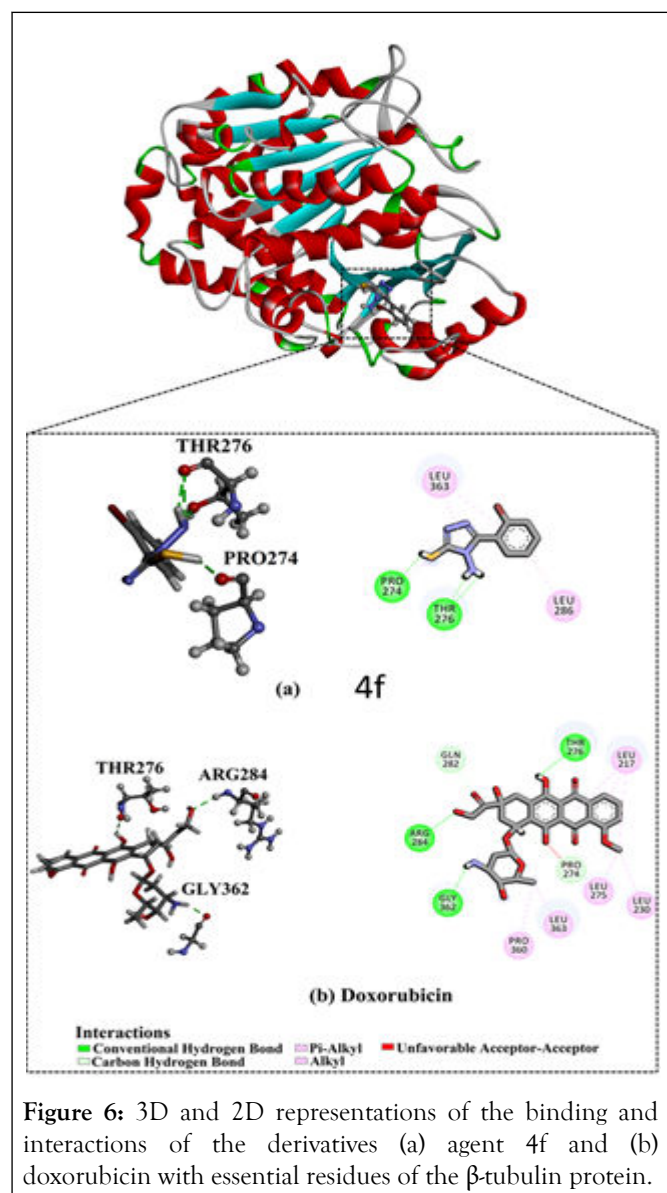


**Figure 6:** 3D and 2D representations of the binding and interactions of the derivatives (a) agent 4f and (b) doxorubicin with essential residues of the  $\beta$ -tubulin protein.

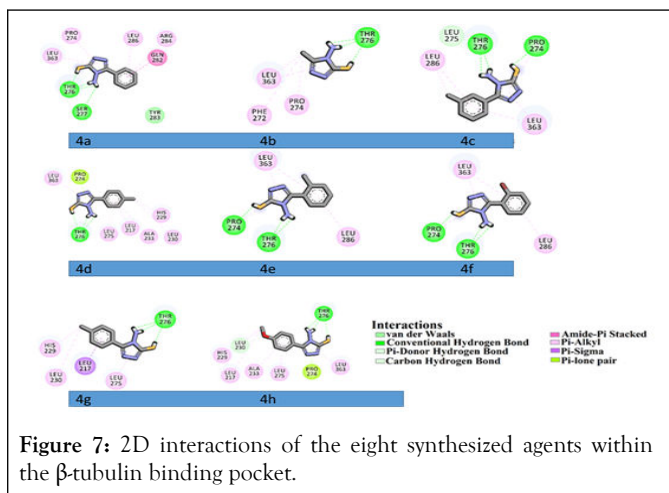
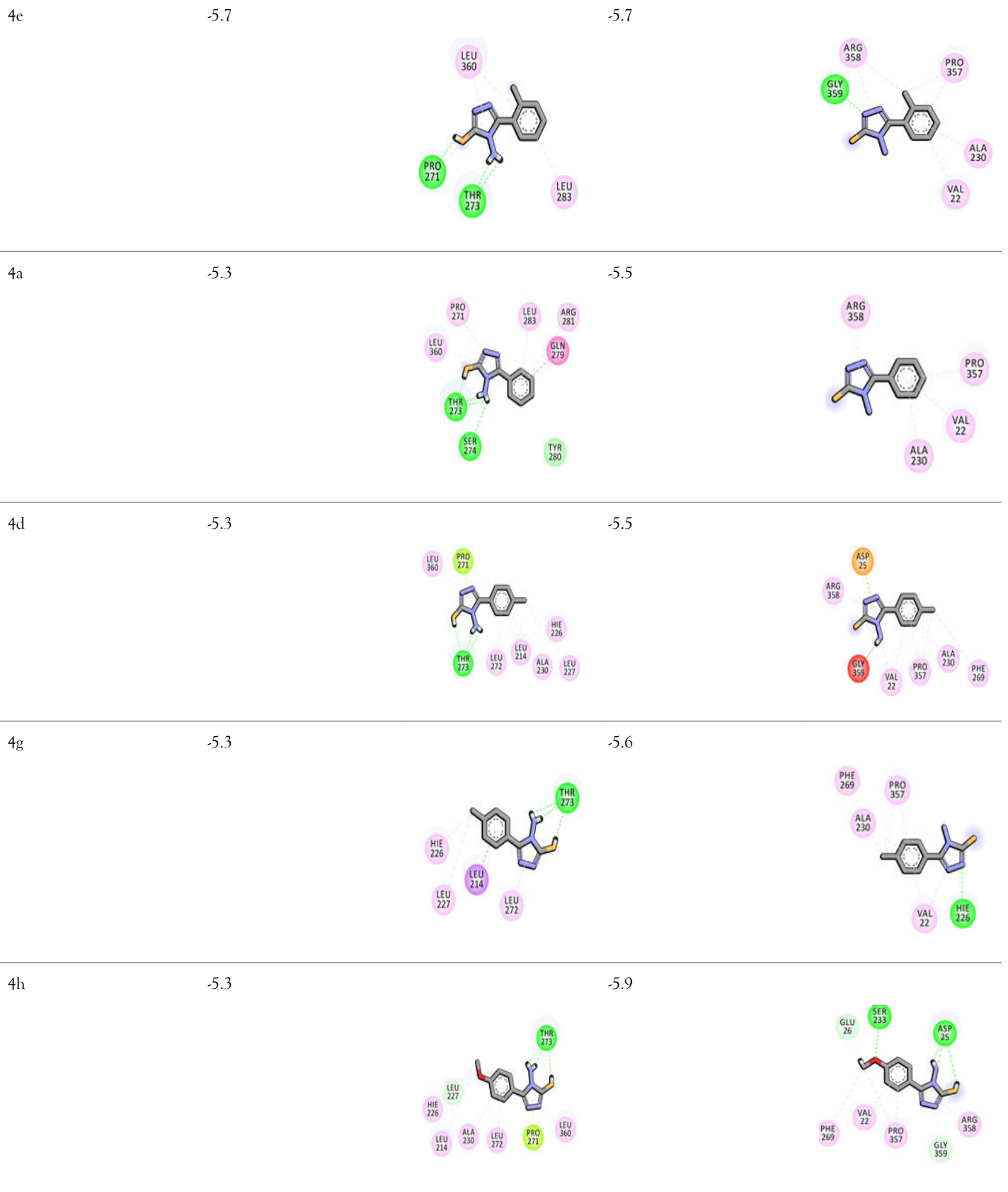


**Table 8:** The docking score of the 1,2,4-triazole derivatives against the  $\beta$ -tubulin protein compared with doxorubicin.

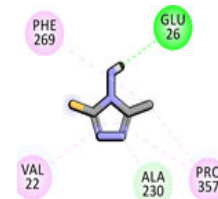
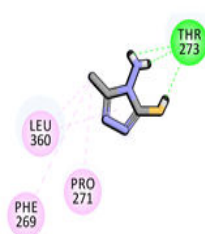
Agent	Auto-dock (Docking score kcal/mol)	2D interactions	Vina (Docking score kcal/mol)	2D interactions
Doxorubicin	-6.8		-8	
4f	-5.9		-5.6	
4c	-5.8		-5.7	



4b

-3.7

-3.8



Note: The 1,2,4-triazole agents categorized from the most potent to least potent agent

**Table 9:** Computed docking scores (kcal/mol) and features for eight synthesized compounds and doxorubicin against the  $\beta$ -tubulin protein.

Agent name	Docking score (kcal/mol)	Binding features (hydrogen bond length in Å)
4f	-5.9	THR276 (2.16, 2.47, 2.07 Å), PRO274 (2.08 Å)
4c	-5.8	THR276 (2.13, 2.10 Å), PRO274 (2.05 Å)
4e	-5.7	THR276 (2.17, 2.49, 2.08 Å), PRO274 (2.07 Å)
4a	-5.3	THR276 (2.27, 2.20, 2.63, 2.00 Å), SER277 (2.84 Å)
4d	-5.3	THR276 (2.14, 2.12, 2.12 Å)
4g	-5.3	THR276 (2.65, 2.12, 2.10, 2.24 Å)
4h	-5.3	THR276 (2.14, 2.12, 2.18 Å)
4b	-3.7	THR276 (1.97, 1.93, 2.07, 2.58 Å)
Doxorubicin <sup>a</sup>	-6.8	THR276 (2.37 Å), ARG284 (2.22 Å), GLY362 (1.97 Å)

Note: <sup>a</sup>Positive control. The data reported from the best scores

## DISCUSSION

The 1,2,4-triazole core is an important scaffold to design anticancer agents and received considerable attention these days. 1,2,4-triazole scaffold possesses an important physicochemical property that improves the solubility, bioavailability and chemical stability of the molecule. This scaffold is polar and can increase the solubility of the ligand and improve the pharmacological profile showing hydrogen bond acceptor, donor and hydrophobic interactions. Therefore, in this research, SAR was applied and positions three and four were fixed with thiol and amino groups because of their biological anticancer activities and change the moieties only in the R position. Also, It was found that the aromatic nature of triazole makes it resistant to metabolic degradation, acid-base hydrolysis and redox conditions. Furthermore, studies showed that aromatic moiety is important for anti-tumor activity. Besides the

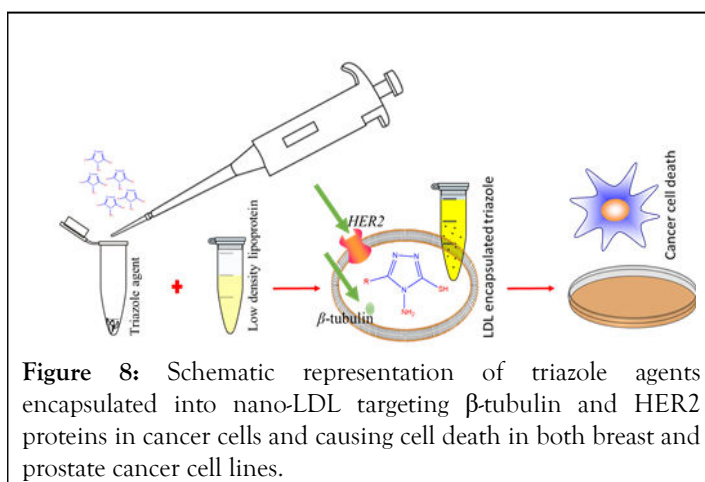
anticancer activity, methoxy substituent showed antibacterial activity, while triazole thions possess anti-convulsant activity. Moreover, recently triazole derivative with bromo-phenyl moiety has shown potent anticancer activities against aggressive cancer models. Another finding is triazole agent that holds hydrogen bonding in the para position possesses good inhibitory activity. Triazole agents have chloro, bromo, methyl and methoxy, in ortho, meta or para position showing strong anticancer activities.

Furthermore, the nano-size and shape of the eight agents increased the effect of cancer cell death. A study used PEGylated graphene oxide sheets for breast cancer therapy. Other studies used titanium diselenide nanosheets and the data showed enhancement in photocatalytic therapy and apoptosis in cancer cells. Further, liposomal doxorubicin-graphene nanosheets were used against the MCF7 cancer cell line and the results were promising. Moreover, silica nanoparticles of rode-like

morphology showed anticancer activities. In addition, many types of nano-rods particles were studied such as gold, silver, carbon, zinc, iron oxide, tin oxide, copper oxide and silica nanorods had biological activities. These nanoparticles either the sheets or the rods disturbed the dimerization of HER2 protein in the extracellular domain and disrupted the downstream signaling pathways, also disrupted the  $\beta$ -tubulin activity during the cell division to two daughter identical cells leading in both cases to mitosis and cancer cell death [17].

After that, triazole derivatives were encapsulated into nano-LDL particles and the particle sizes became bigger and the new absorbance peaks appeared because the agents were embedded in the LDL particles. In addition, the presence of one absorption peak for each sample indicated the symmetrical geometry and formulation for all LDL particles encapsulated with the triazole agents. The shift observed in LDL particles encapsulated with triazole agents could be attributed to the difference in the agent's shape and size distribution. It is obvious that the presence of the nano-LDL particles around the agent enhances its thermal stability yield as shown in the thermal gravimetric analysis [18].

A previous study showed that triazole hybrids showed anti-proliferation activities in A549, Panc1, HT29 MCF7 cell line through the EGFR signaling pathway. Moreover, a research study proved that 1,2,4-triazole derivatives demonstrated significant anti-proliferation activity against MCF7 and PC3 cell lines. In addition, a study proved that the 1,2,4-triazole core has biological anti-proliferation activity against both DU145. Abbas and Dawood, proved that triazole hybrids had potent activity toward MCF7 and MDA468 cell line. In western blot analysis, The data proved that MDA468 does not express HER2 receptor protein therefore the triazole agents targeted the DU145 which is the HER2-positive cell line. In sum, an active drug delivery strategy was used by encapsulating nano triazole derivatives into nano-LDL particles which bind to the LDL-receptor and internalize into cancer cells and cause its death proved in the DU145 prostate cancer cell line, as shown in Figure 8 [19].



The *in-silico* investigations showed that all the designed triazole agents showed good binding with  $\beta$ -tubulin protein in both cell lines. Doxorubicin anticancer drug, positive control and with a great docking score a value of  $-6.8$  kcal/mol was used to compare with our designed triazoles. Doxorubicin demonstrated three

hydrogen bonds with THR276 (2.37 Å), ARG284 (2.22 Å) and GLY362 (1.97 Å). A docking comparison of doxorubicin with triazole agent 4f manifested competing docking scores suggesting the *in-silico* potency of agent 4f as a  $\beta$ -tubulin protein inhibitor. Studies proved that triazole derivatives showed hydrogen bonds and hydrophobic interactions with  $\beta$ -tubulin docking study [20].

## CONCLUSION

In conclusion, a new class of triazole derivatives was synthesized, characterized and screened for anticancer activity using an active targeting strategy and proved by docking study. The nano-sheets, nano-rods structures and the nano-size particles of the triazole derivatives were important factors that affected biological activity and disrupt the cell division. *In-vitro* biological evaluation of the 1,2,4-triazole derivatives with the tested cell line showed strong anticancer activity before and after nano-LDL particle encapsulations. In sum, agent 4f structure was confirmed by x-ray single crystal and it exhibited potent anticancer activity due to the chloride substituted on the ortho position on the benzene ring. Western blot assessment showed that DU145 is HER2 positive cell line while MDA468 is HER2 negative cell line. This means the triazole agents caused cell death by targeting both HER2 receptor protein and  $\beta$ -tubulin only in the DU145 cell line. Therefore, in both cell lines, the docking scores and poses of the synthesized agents against  $\beta$ -tubulin protein were demonstrated utilizing AutoDock4.2.6 software. Agent 4f scores revealed an eminent against the  $\beta$ -tubulin protein in both cell lines MDA468 and DU145. These findings highlighted the significance of agent 4f as a prospective anticancer agent. In conclusion, taking the above information into account, we can summarize that nano-LDL particles encapsulated 1,2,4-triazoles derivatives enter the DU145 cancer cells by binding to the LDL receptor and serving as an active drug delivery platform and revealing promising anticancer results. While MDA468 cell proliferation was targeted through  $\beta$ -tubulin only. In conclusion, the 1,2,4-triazoles are confirmed to be the building blocks for potent biologically active agents.

## ACKNOWLEDGMENT

The author of this work is very grateful to both Kuwait University-Research sector and Cleveland Clinic for providing all the facilities to conduct this project. In addition, we acknowledge project numbers (GS01/01, GS01/03, GS01/05, GS02/01, GS03/08) at Kuwait University. In addition, I would like to thank Dr. Mayada Samir for analyzing the TGA data. In addition, special thanks to the Nanoscopy Science Center at Kuwait University for performing the triazole agent's morphology images.

## DISCLOSURE STATEMENT

No potential conflict of interest was reported by the author.

## FUNDING

All this work was supported by grant number SC03/23 from Kuwait University-Research Sector.

## REFERENCES

1. Abdellatif AA. A plausible way for excretion of metal nanoparticles *via* active targeting. *Drug Dev Ind Pharm.* 2020;46(5):744-750.
2. Abdellatif AA, Alturki HN, Tawfeek HM. Different cellulosic polymers for synthesizing silver nanoparticles with antioxidant and antibacterial activities. *Sci Rep.* 2021;11(1):84.
3. Ahuja R, Sidhu A, Bala A, Arora D, Sharma P. Structure based approach for twin-enzyme targeted benzimidazolyl-1, 2, 4-triazole molecular hybrids as antifungal agents. *Arab J Chem.* 2020;13(6):5832-5848.
4. Ajmal M, Yunus U, Graham RM, Leblanc RM. Design, synthesis and targeted delivery of fluorescent 1, 2, 4-triazole-peptide conjugates to pediatric brain tumor cells. *ACS Omega.* 2019;4(27):22280-22291.
5. Alhadad LJ, Harisa GI, Alanazi FK. Design and encapsulation of anticancer dual HSP27 and HER2 inhibitor into low density lipoprotein to target ovarian cancer cells. *Saudi Pharm J.* 2020;28(4):387-396.
6. Jaragh-Alhadad LA, Harisa GI, Alanazi FK. Development of nimesulide analogs as a dual inhibitor targeting tubulin and HSP27 for treatment of female cancers. *J Mol Struct.* 2022;1248:131479.
7. Ali A, Al-Hassani R, Hussain D, Jabir M, Meteab H. Anti-proliferative activity and tubulin targeting of novel micro and nanoparticles complexes of 4-amino-3-thion-1, 2, 4-triazole derivatives. *Nano Biomed Eng.* 2020;12(1).
8. Aouad MR, Al-Mohammadi HM, Al-Blewi FF, Ihmaid S, Elbadawy HM, Althagfan SS, et al. Introducing of acyclonucleoside analogues tethered 1, 2, 4-triazole as anticancer agents with dual epidermal growth factor receptor kinase and microtubule inhibitors. *Bioorg Chem.* 2020;94:103446.
9. Bharadwaj S, Dubey A, Kamboj NK, Sahoo AK, Kang SG, Yadava U. Drug repurposing for ligand-induced rearrangement of Sirt2 active site-based inhibitors *via* molecular modeling and quantum mechanics calculations. *Sci Rep.* 2021;11(1):10169.
10. Carrion-Salip D, Panosa C, Menendez JA, Puig T, Oliveras G, Pandiella A, et al. Androgen-independent prostate cancer cells circumvent EGFR inhibition by overexpression of alternative HER receptors and ligands. *Int J Oncol.* 2012;41(3):1128-1138.
11. Dehestani L, Ahangar N, Hashemi SM, Irannejad H, Masihi PH, Shakiba A, et al. Design, synthesis, *in vivo* and *in silico* evaluation of phenacyl triazole hydrazones as new anticonvulsant agents. *Bioorg Chem.* 2018;78:119-129.
12. Ding Y, Guo H, Ge W, Chen X, Li S, Wang M, et al. Copper (I) oxide nanoparticles catalyzed click chemistry based synthesis of melampomagnolide B-triazole conjugates and their anti-cancer activities. *Eur J Med Chem.* 2018;156:216-229.
13. Ding M, Wan S, Wu N, Yan Y, Li J, Bao X. Synthesis, structural characterization and antibacterial and antifungal activities of novel 1, 2, 4-triazole thioether and thiazolo (3, 2-b)-1, 2, 4-triazole derivatives bearing the 6-fluoroquinazoliny moiety. *J Agric Food Chem.* 2021;69(50):15084-15096.
14. Duo Y, Luo G, Li Z, Chen Z, Li X, Jiang Z, et al. Photothermal and enhanced photocatalytic therapies conduce to synergistic anticancer phototherapy with biodegradable titanium diselenide nanosheets. *Small.* 2021;17(40):2103239.
15. Fallah Z, Isfahani HN, Tajbakhsh M, Mohseni M, Zabihi E, Abedian Z. Antibacterial and cytotoxic effects of cyclodextrin-triazole-titanium based nanocomposite. *Braz Arch Biol Technol.* 2021;64:e21190750.
16. Gao F, Wang T, Xiao J, Huang G. Antibacterial activity study of 1, 2, 4-triazole derivatives. *Eur J Med Chem.* 2019;173:274-281.
17. Gasteiger J, Marsili M. Iterative partial equalization of orbital electronegativity-a rapid access to atomic charges. *Tetrahedron.* 1980;36(22):3219-3228.
18. Goodford PJ. A computational procedure for determining energetically favorable binding sites on biologically important macromolecules. *J Med Chem.* 1985;28(7):849-857.
19. Grytsai O, Valiashko O, Penco-Campillo M, Dufies M, Hagege A, Demange L, et al. Synthesis and biological evaluation of 3-amino-1, 2, 4-triazole derivatives as potential anticancer compounds. *Bioorg Chem.* 2020;104:104271.
20. Ye H, Wang J, Wang N, Wu D, Li H, Geng F. Ultrasound-assisted pH-shifting remodels egg-yolk low-density lipoprotein to enable construction of a stable aqueous solution of vitamin D3. *Curr Res Food Sci.* 2022;5:964-972.